The influence of ambipolar diffusion on the attachment length and electron temperature in orificed hollow cathodes

IEPC-2019-A628

Presented at the 36th International Electric Propulsion Conference
University of Vienna, Austria
September 15–20, 2019

Pierre-Yves C. R. Taunay,*
Princeton University, Princeton, NJ, 08544, U.S.A.
and
Christopher J. Wordingham†
Princeton University, Princeton, NJ, 08544, U.S.A.
and
Edgar Y. Choueiri‡
Princeton University, Princeton, NJ, 08544, U.S.A.

The mechanism controlling the scaling of the electron temperature and attachment length within orificed hollow cathodes is investigated numerically by combining a theoretical zero-dimensional plasma flow model and a charge-exchange-limited ambipolar diffusion model. Electron temperature and attachment length are critical because they determine the effective utilization, and therefore the operational life, of thermionic hollow cathode inserts. Conservation of momentum for the combined-species flow, conservation of energy for the electrons, and the assumption of charge-exchange-limited ambipolar diffusion are used to derive the underlying models. The combined model takes as inputs the operating conditions (discharge current and mass flow rate), cathode geometry, and the gas species, along with two non-controllable parameters: the neutral gas temperature and the sheath potential. Good agreement with experimental data is obtained for the emission length and electron temperature, both as functions of the neutral gas pressure-insert diameter product, and as functions of discharge current. Both the zero-dimensional model and the experimental data show that orificed cathodes operate in the region of neutral gas pressure-diameter product $P \cdot d \approx 1$ Torr-cm. The predicted emission length is found to be between 0.8 and 1.2 times the insert radius, to scale weakly with the pressure-diameter product, and to be nearly independent of the orifice diameter. The analysis also suggests that the diffusion-dominated nature of the insert plasma can account for the scaling of the emission length with cathode operating conditions.

List of Symbols

Constants			d_c	Cathode (insert) diameter	m
k_B	Boltzmann's constant	1.38×10^{-23} J/K	L_{emit}	Emission length	m
Geometry			L_o	Orifice length	m
$\bar{r}_o$	Orifice radius normalized to insert radius		r_c	Cathode (insert) radius	m

*Graduate Research Assistant, EPPDyL; MAE Dept., Princeton University, ptaunay@princeton.edu.
†Graduate Student, EPPDyL; MAE Dept., Princeton University, cjw4@alumni.princeton.edu.
‡Chief Scientist, EPPDyL, Professor, Applied Physics Group, MAE Dept., Princeton University.

r_o	Orifice radius	m	T_{eV}	Electron temperature	V
Plasma parameters			**Flow properties**		
n_e	Electron density	m^{-3}			
n_g	Neutral gas density	m^{-3}	P	Total pressure	Pa
T_g	Neutral gas temperature	K	P_g	Neutral gas pressure	Pa

I. Introduction

THE next-generation of Hall and ion thrusters will require more demanding discharge currents and operational lifetimes than are presently available. Discharge powers for "near-term" thrusters are in the range of 100 to 200 kW,[1] with expected mission lifetimes of up to 100 kh.[2,3] These requirements translate to up to 700 A of required discharge current for a specific impulse in the range of 2000 to 6000 s.[4] Life tests of up to 50 kh have been performed for low-discharge-current cathodes (less than 4 A).[5] High-discharge-current cathodes have been successfully operated in the 300–400 A range[6,7] with estimated lifetimes of nearly 12 kh at 100 A.[8] Life tests are time-consuming and costly so there is a clear need for models that can accurately estimate the operational life of thermionic hollow cathodes.

Because the temperature of the thermionic emitter, which controls its evaporation rate, is dependent on the effective emission area, the insert electron temperature and the "attachment length" are of the utmost importance. The attachment length is the length over which the internal plasma is sufficiently dense to support temperature-limited thermionic emission. Both parameters also govern the power deposition from the plasma to the emitter. Using the charge-exchange-limited ambipolar diffusion model described in Ref. 9, it can be shown that both quantities depend primarily on the product of the diameter and the neutral density for a variety of operating conditions. We have developed[10] semi-analytical correlations for both electron temperature and attachment length in argon- and xenon-fed hollow cathodes using the results of this model. These correlations remain to be verified experimentally.

Both the electron temperature and plasma density profile(s) can be measured using a scanning Langmuir probe as shown in Refs. 11–14. The attachment length can be inferred directly from the plasma density profile in the insert plasma region. In this work we compare the theoretical correlations, developed using the ambipolar diffusion model, to available experimental data for a few cathodes. We first briefly present the theoretical framework, then explain the data analysis methodology, and finally compare the theoretical results to experimental data.

II. Approach

A. Numerical models

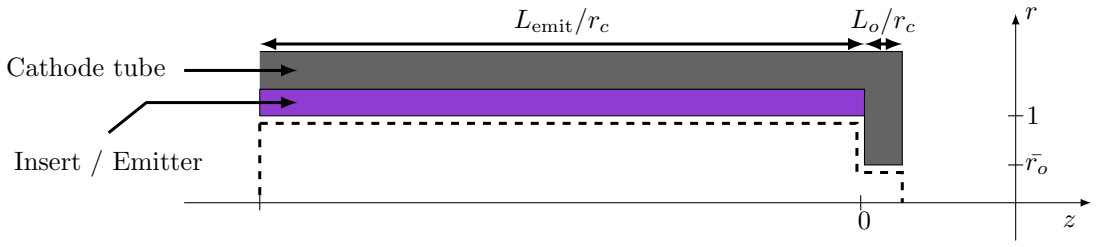

Figure 1: Fluid control volume considered in the analysis.

We consider the fluid control volume shown in Fig. 1 and use both the ambipolar diffusion model presented in Ref. 9 and the zero-dimensional model of the insert and orifice regions presented in Ref. 10. Both models feature common assumptions:

1. The plasma density is governed by charge-exchange-limited ambipolar diffusion,

2. The Bohm flux is not modified by the presence of an emitting sheath,

3. The electron temperature is constant in each (insert/orifice) region, and

4. The heavy particle temperature is constant within the cathode and is a free parameter.

These assumptions are typically valid in the orificed hollow cathodes that we consider. Further discussion of the assumptions can be found in Refs. 9, 10.

The ambipolar diffusion model permits the calculation of both the plasma density profile and the electron temperature in the insert region of a hollow cathode. The details of the model and algorithm are presented in Ref. 9 and are not repeated here. The solution to the ambipolar diffusion equation for the plasma density has the following form:

$$n_e\left(\bar{r},\bar{z}\right) = \sum_{k=1}^{+\infty} C_k J_0\left(\lambda_k \bar{r}\right) \exp\left(\alpha_k \bar{z}\right), \tag{1}$$

where $\bar{r}$ and $\bar{z}$ are the spatial coordinates normalized by the insert radius, C_k is the coefficient of the k^{th} eigenmode, J_0 is the 0^{th} order Bessel function of the first kind, and λ_k and α_k are the eigenvalues and separation constant, respectively. The expressions for C_k, λ_k, and α_k are also given in Ref. 9.

Because the separation constant α_k increases with k, the first-order eigenmode dominates as $\bar{z} \to -\infty$. We therefore define the attachment length as the decay-length scale of the first-order eigenmode of the 2D solution in the insert region. This corresponds to the length scale of the exponential electron density decay in the upstream region of the cathode insert:

$$L_{\text{emit}} = \frac{r_c}{\alpha_1}. \tag{2}$$

The assumption we made in Ref. 9 that the net ion flux is zero on the orifice inlet plane implies that the plasma density resulting from the algorithm always features a peak at the orifice inlet and likely represents a lower bound for the attachment length. This assumption is generally acceptable for cathodes with small orifice-to-insert diameter ratio. The true attachment length, however, will likely be larger than that predicted by the algorithm for cathodes with either larger orifices or no orifice, or for cathodes operated at low mass flow rates or at low internal pressures. For these cathodes the peak in the electron density profile is typically situated upstream from the orifice inlet.

We combined the ambipolar diffusion model with the 0-D model we developed in Ref. 10 in order to compute volume-averaged plasma properties and to provide the neutral gas pressure or density prediction required by the ambipolar diffusion model. The 0-D model is based on a rigorous treatment of the plasma-neutral flow through the cathode orifice but requires the electron temperature and emission length, as calculated by the ambipolar diffusion model, to close the system. The 0-D approach combines the plasma fluid equations for the plasma-neutral flow and the electron energy equation in both insert and orifice regions. In this work, we calculate the neutral gas density in order to predict both experimental emission length and electron temperature as functions of the neutral gas pressure-diameter product.

B. Comparison to experimental data

Dataset We use the electron temperature and plasma density profiles measured for the following cathodes:

- Salhi's cathode[15] operating on xenon at a mass flow rate of 0.5 equivalent-Ampères,
- the NSTAR discharge cathode,[12]
- the NEXIS discharge cathode,[16] and
- the JPL 1.5 cm LaB_6 cathode.[17]

For the calculation of the total pressure-diameter product presented in the last section of this paper, we use measured pressure data from the following cathodes:

- Siegfried and Wilbur's mercury cathode,[18]
- Friedly's cathode,[19]
- Salhi's cathode[15] operating on both argon and xenon,

- the T6 cathode,[20,21]
- Domonkos's cathodes (AR3, EK6, SC012),[22]
- the NSTAR discharge cathode,[23,24]
- the NEXIS cathode,[13,25] and
- Princeton's large hollow cathode.[10]

Attachment length The experimental attachment length is derived from the measurement of the electron density profile. Because we define the attachment length as the length-scale of the exponential decay of the electron density upstream of the cathode orifice, we fit only the relevant portion of the experimental data with a decaying exponential. We show an example of this approach in Fig. 2.

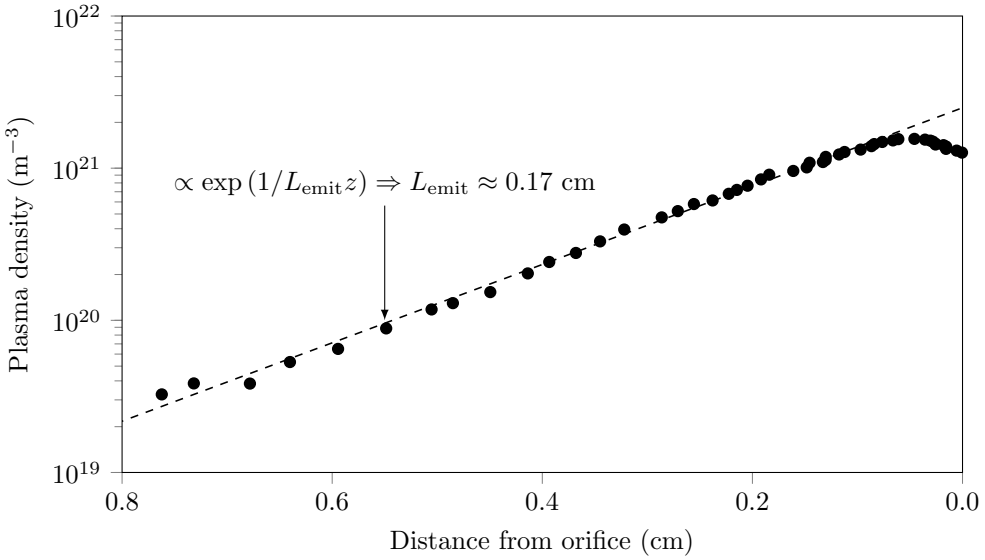

Figure 2: Example of the derivation of the attachment length from an electron density profile. Experimental data from Ref. 12 for the NSTAR discharge cathode operating at 15 A.

The NSTAR, NEXIS, and JPL LaB_6 cathodes share the same experimental setup and diagnostics for which the error in the density measurement was reported[26] to be $\pm 40\%$ ($\sigma_n^2 = 0.04$). For the density measurements taken by Salhi no experimental uncertainty was reported so we assume the same value of $\pm 40\%$. The error inherent in performing the various steps of the linear regression on the logarithm of the density must also be estimated to obtain a confidence interval for the derived attachment length. If the density at a given point has a variance of $\bar{n}_e^2 \sigma_n^2$ (where $\bar{n}_e$ is the average density at that point) then its logarithm $Y = \ln n_e$ has a variance of σ_n^2. We derive this property in the Appendix. For the linear fit of $\ln n_e$ with parameters $\hat{\beta}_0$ and $\hat{\beta}_1$, we have

$$\hat{Y} = \hat{\beta}_0 + \hat{\beta}_1 \bar{z}. \tag{3}$$

The inverse of $\hat{\beta}_1$ is the normalized emission length. The standard error of the slope is:[27]

$$\sigma_\beta^2 = \frac{\sigma_n^2}{\sum_{i=1}^{N} (\bar{z}_i - \hat{z})^2}, \tag{4}$$

where $\hat{z}$ is the average distance from the orifice inlet. If we now assume that $\hat{\beta}_1$ is also normally distributed about the value calculated using the regression procedure, then the emission length has a variance (to first order) of

$$\sigma_L^2 = \frac{\sigma_\beta^2}{\hat{\beta}_1^2}. \tag{5}$$

We also give the derivation for the variance of the inverse of a normally distributed random variable in the Appendix.

Electron temperature The electron temperature is typically measured as a function of position in the insert region. Because the electron temperature typically varies gradually upstream of the cathode orifice, we use the axial line-average of the experimental data over the entire cathode insert region to obtain a single experimental value. We take the uncertainty of the electron temperature measurements to be ± 0.5 eV, as reported in Ref. 26, unless otherwise specified.

Methodology With the ambipolar diffusion model, we compute the numerical values of the attachment length and electron temperature as functions of the neutral gas pressure and orifice-to-insert diameter ratios. The results of the ambipolar diffusion model are combined with the 0-D model to compute the plasma parameters for a variety of experimental operating conditions (discharge current, mass flow rate, cathode geometry, and gas species). For each experimentally-measured data point we compute

1. the neutral gas pressure using the 0-D model, and
2. an estimate of both attachment length and electron temperature using the ambipolar diffusion model.

The combination of the calculated neutral gas pressure and the experimentally-measured electron temperature and attachment length are compared to the resulting values of the ambipolar diffusion model as functions of pressure-diameter product. We separately compare the estimate of the attachment length and electron temperature calculated from the combined models to their experimentally-measured counterparts as functions of discharge current.

III. Results and discussion

We have found that both attachment length and electron temperature are sensitive only to the neutral gas density-insert diameter product for the range of values considered. For a constant heavy particle temperature this corresponds to the neutral pressure-diameter product. We have derived the following semi-analytical expressions for both electron temperature,

$$T_{eV}^{\text{insert}} = \frac{t_{i,0}}{(P_g d_c)^{t_{i,1}}} + t_{i,2}, \tag{6}$$

and attachment length,

$$L_{\text{emit}} = \frac{d_c}{2}\left(l_0 + \frac{l_1}{\ln^6\left(P_g d_c + l_2\right)}\right), \tag{7}$$

respectively, by fitting the results of the ambipolar diffusion model as functions of the pressure-diameter product and the ratio of orifice to insert diameter to the functional forms given above. d_c and $P_g = n_g k_B T_g$ are the insert diameter and the neutral gas pressure, respectively. The coefficients $t_{i,k}$ and l_k for xenon and argon gases are given in the Appendix. In all cases, the pressure-diameter product that appears in the denominator is in Torr-cm.

In Figs. 3 and 4 we show the attachment length and electron temperature as calculated using the ambipolar diffusion model (Eqns. 6 and 7) and the combined 0D model from Ref. 10, respectively. We compare the model results to experimental data in the dataset described above for orificed hollow cathodes operating on xenon gas. Results are shown as a function of the neutral gas pressure-diameter product for the ambipolar diffusion model and as a function of discharge current for the 0D model. We obtain good agreement between models and experimental data, which suggests that the models are capable of capturing the appropriate physics.

Attachment length Figure 3 shows that the attachment length varies between 0.8 and 1.2 times the cathode insert radius and scales weakly with the pressure-diameter product. As defined, it is insensitive to the orifice diameter, as suggested experimentally.[29] We also show in Fig. 3 the previous empirically-derived scaling relationship suggested in Ref. 28:

$$L_{\text{emit}} = K/P, \tag{8}$$

where K is a constant between 5–15 Pa-m. We plot the results using the neutral gas pressure (as opposed to the total pressure). A similar expression to Eqn. 8 can be derived using the results from the electron

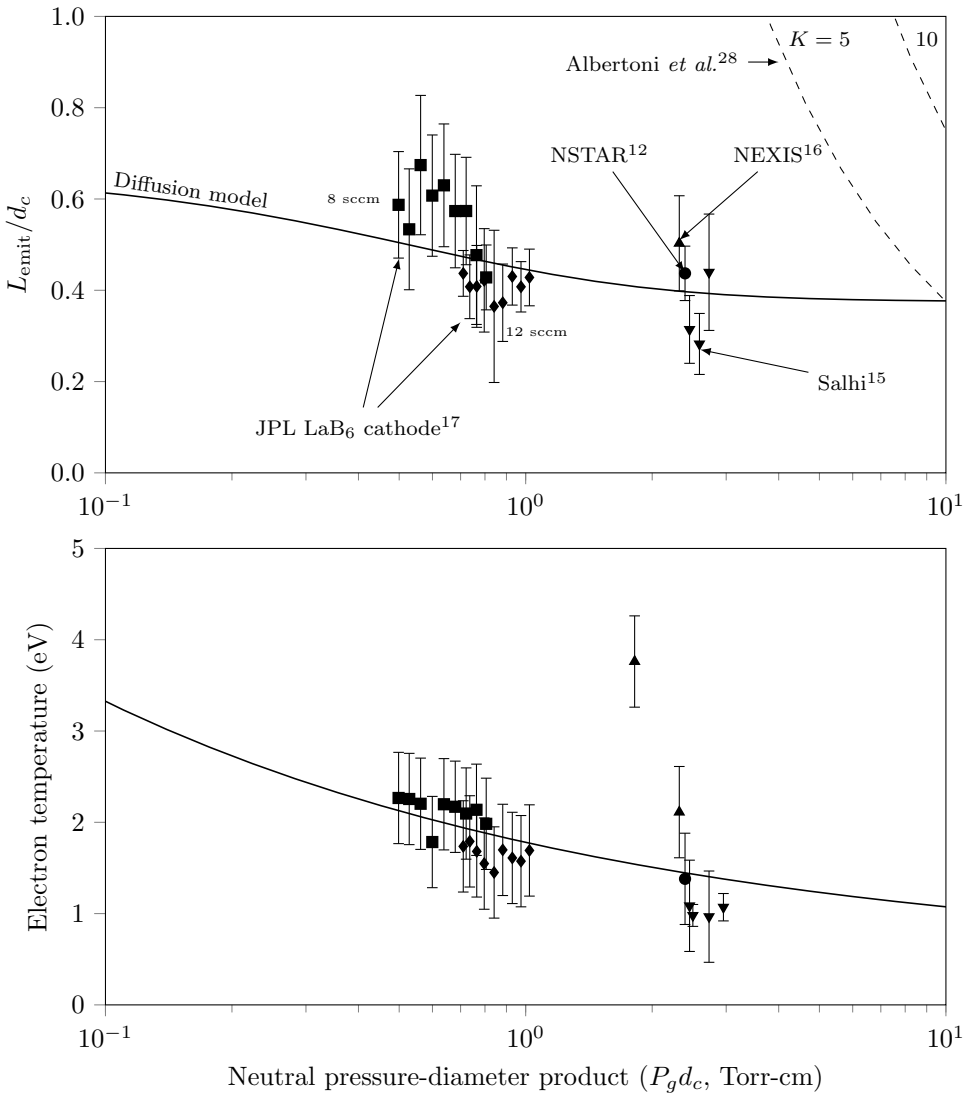

Figure 3: Attachment length (top) and electron temperature (bottom) as functions of the neutral pressure-diameter product.

transport approach of Ref. 30 if one considers sheath voltages less than 8 V for xenon. The corresponding constant is between 0.01–15 Pa-m for ionization fractions between 0.1% and 10% and sheath potentials between 1 and 8 V.

The observed scaling of attachment length cannot be captured by the electron transport phenomena suggested in Ref. 30, nor by the purely empirical relationship given in Ref. 28 (which does not offer a mechanistic explanation). The results of the ambipolar diffusion model suggest that the observed behavior is governed not by the total static pressure but by the *neutral gas* pressure. When supplied with the neutral gas pressure estimation of the 0-D model, the plasma density decay predicted by the ambipolar diffusion model appears to account for the variation of the observed attachment length.

Pressure-diameter product Most of the experimental data is clustered around a measured (total static) pressure-diameter product of $Pd \approx 1$ Torr-cm. Because the insert neutral pressure is always less than the total pressure, the *total* pressure-diameter product gives an upper bound on the neutral pressure-diameter product. This value has been observed to be a sufficient condition for the efficient operation of tube cathodes on a variety of gases.[31,32] Similar observations have been made for orificed hollow cathodes that operate with mercury[33] and noble gases.[34]

We show in Fig. 5 the statistical distribution of the total pressure-diameter product for the pressure

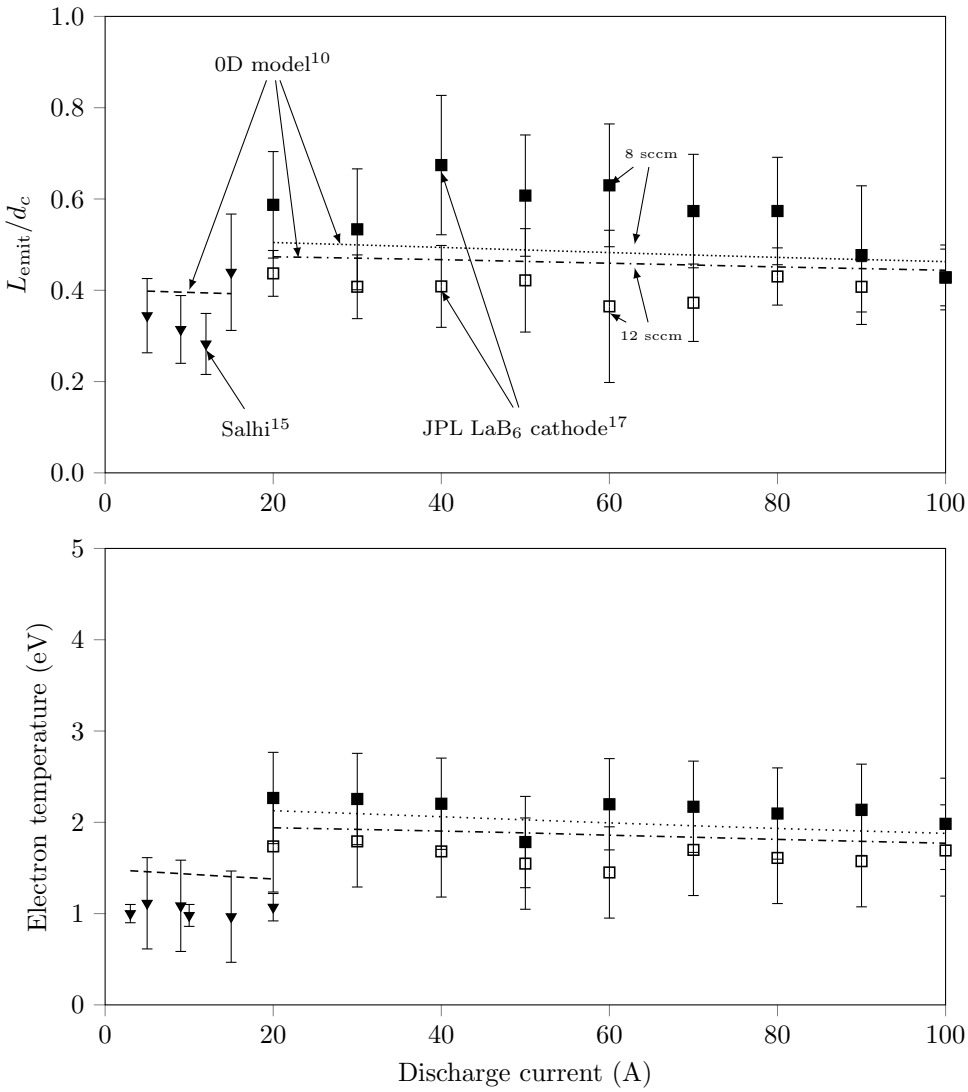

Figure 4: Attachment length (top) and electron temperature (bottom) as functions of discharge current.

dataset described in Section II.B. The dataset has roughly 400 operating points and includes data for argon, xenon, and mercury. The distribution is shown both as a histogram with 40 bins and as a density function obtained with the Kernel Density Estimation (KDE) technique. We use a Gaussian kernel for the KDE with an optimum bandwidth that is found using a grid search with cross-validation. The KDE method, grid search, and cross-validation are implemented in the Python library `scikit-learn`.[35] Due to the decaying nature of the solutions to the ambipolar diffusion equation, for the very high total pressures (164–609 Torr) measured in cathodes from Ref. 22 we expect that the peak plasma density occurs in the orifice as opposed to the insert. To reflect this, we show in Fig. 5b the pressure-diameter product where we have used the orifice diameter for the cathodes presented in Ref. 22 and the insert diameter for all other cathodes. We see that the operation of cathodes is distributed mostly in a region where the pressure-diameter product is 10 Torr-cm or less. The most probable pressure-diameter is 4.2 Torr-cm.

We emphasize that the *local neutral* pressure, as opposed to the one measured upstream of the cathode, should be used to determine the pressure-diameter product. In the absence of direct experimental measurements of the local neutral pressure, we can only estimate this product from the total upstream pressure. For cathodes that are operating at a high ($\geq$ 10 Torr-cm) total pressure-diameter product, it is likely that the peak electron density is near the cathode orifice. In these cases, we expect the rapid pressure drop due to the flow constriction near the orifice results in a pressure-diameter product near the most probable value

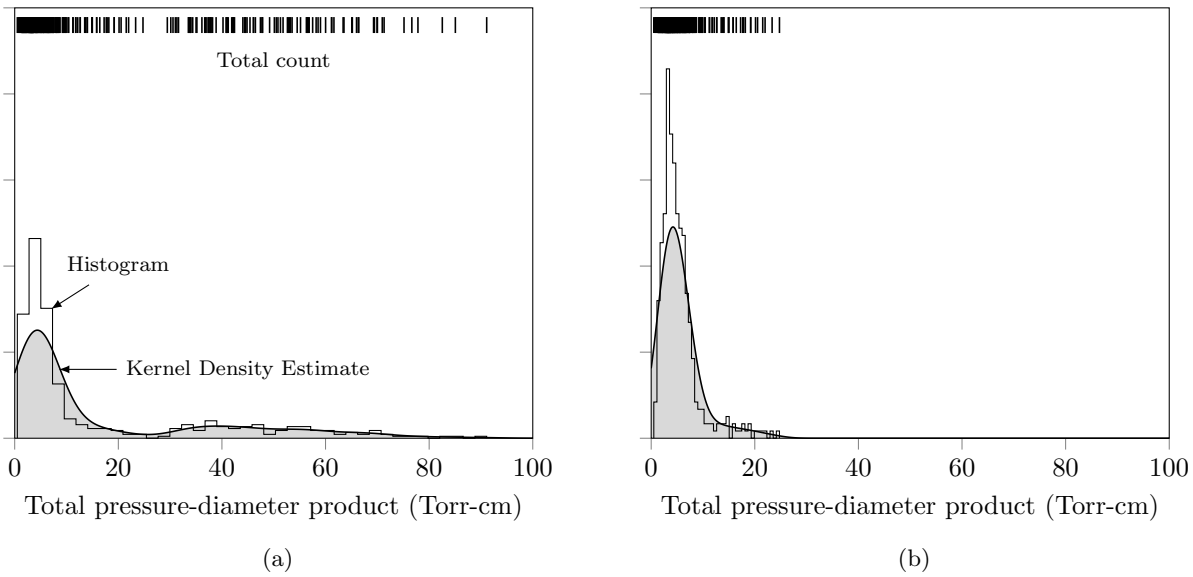

Figure 5: Distribution of total pressure-diameter product for a large number of cathodes. Left: Pressure-diameter product calculated using the insert diameter for all cathodes. Right: Pressure-diameter product calculated using the orifice diameter for only those cathodes presented in Ref. 22.

close to or inside the orifice.

IV. Conclusion

Using the combination of our previous modeling efforts presented in Refs. 9 and 10 we have computed the attachment length and electron temperature for a variety of operating conditions. As noted in Ref. 10, we have found that both quantities vary only with the neutral pressure-diameter product. Despite neglecting the variation of several properties in the insert region we find good agreement between experimental results gathered from the literature and the semi-analytical fits calculated by the model. This suggests that the ambipolar diffusion model in combination with the pressure predictions of the zero-dimensional model captures the relevant physics that govern the scaling of the attachment length and electron temperature.

The charge-exchange-limited ambipolar diffusion model relies on the assumption of a peak density at the orifice inlet and therefore can only give an estimate of the attachment length through the exponential density decay length scale. This is an acceptable approximation for cathodes with small orifice-to-insert diameter ratio. The true attachment length may be larger but the inclusion of the appropriate near-orifice effects would add significant complexity to the model. As we have noted previously in Ref. 10, the two free parameters of the 0-D model (sheath potential and neutral gas temperature) could be self-consistently incorporated through a potential solver and the energy equation for the heavy particles, respectively. A potential solver would also allow for the attachment length to be more accurately determined, as the temperature-limited emission region of the emitter may then be properly identified.

This work illuminates the underlying regime of operation of orificed hollow cathodes. The results we present and the preponderance of experimental evidence suggest possible design rules for future cathodes: the insert length should be comparable to the insert radius for optimum emitter usage, and the mass flow rate can be initially estimated such that the pressure-diameter product is near 1 Torr-cm.

Acknowledgments

The authors would like to thank the Princeton Program in Plasma Science and Technology for supporting this work.

References

[1]Brown, D. L., Beal, B. E., and Haas, J. M., "Air Force Research Laboratory High Power Electric Propulsion Technology Development," IEEE Aerospace Conference, 2010.

[2]Goebel, D. M. and Chu, E., "High Current Lanthanum Hexaboride Hollow Cathodes for High Power Hall Thrusters," 32nd International Electric Propulsion Conference, 2011, IEPC-2011-053.

[3]Hofer, R., Randolph, T., Oh, D., Snyder, J., and de Grys, K., "Evaluation of a 4.5 kW Commercial Hall Thruster System for NASA Science Missions," 42nd AIAA/ASME/SAE/ASEE Joint Propulsion Conference & Exhibit, 2006, AIAA-2006-4469.

[4]Plasek, M., Wordingham, C. J., Rojas Mata, S., Luzarraga, N., and Choueiri, E. Y., "Experimental Investigation of a Large Diameter Cathode," 50th AIAA/ASME/SAE/ASEE Joint Propulsion Conference & Exhibit, 2014, AIAA-2014-3825.

[5]Shastry, R., et al., "Status of NASAs Evolutionary Xenon Thruster (NEXT) Long-Duration Test as of 50,000 h and 900 kg Throughput," International Electric Propulsion Conference, 2013.

[6]Wordingham, C. J., Taunay, P.-Y. C. R., and Choueiri, E. Y., "Multiple-Kilowatt-Class Graphite Heater for Large Hollow Cathode Ignition," 51st AIAA/SAE/ASEE Joint Propulsion Conference & Exhibit, 2015, AIAA-2015-4010.

[7]Goebel, D. M., Becatti, G., Reilly, S., Tilley, K., and Hall, S. J., "High Current Lanthanum Hexaboride Hollow Cathode for 20-200 kW Hall Thrusters," 35th International Electric Propulsion Conference, 2017, IEPC-2017-303.

[8]Chu, E., Goebel, D. M., and Wirz, R. E., "Reduction of Energetic Ion Production in Hollow Cathodes by External Gas Injection," Journal of Propulsion and Power, Vol. 29, No. 5, 2013, pp. 1155–1163.

[9]Wordingham, C. J., Taunay, P.-Y. C. R., and Choueiri, E. Y., "Theoretical Prediction of the Dense-Plasma Attachment Length in an Orificed Hollow Cathode," 35th International Electric Propulsion Conference, 2017, IEPC-2017-566.

[10]Taunay, P.-Y. C. R., Wordingham, C. J., and Choueiri, E. Y., "A 0-D model for orificed hollow cathodes with application to the scaling of total pressure," AIAA Propulsion and Energy Forum, 2019, AIAA-2019-4246.

[11]Goebel, D. M., Jameson, K. K., Watkins, R. M., Katz, I., and Mikellides, I. G., "Hollow cathode theory and experiment. I. Plasma characterization using fast miniature scanning probes," Journal of Applied Physics, Vol. 98, No. 11, 2005.

[12]Jameson, K. K., Goebel, D. M., and Watkins, R. M., "Hollow Cathode and Keeper-Region Plasma Measurements," 41st AIAA/ASME/SAE/ASEE Joint Propulsion Conference & Exhibit, 2005, AIAA-2005-3667.

[13]Jameson, K. K., Goebel, D. M., and Watkins, R. M., "Hollow Cathode and Thruster Discharge Chamber Plasma Measurements Using High-Speed Scanning Probes," 29th International Electric Propulsion Conference, 2005, IEPC-2005-269.

[14]Goebel, D. M. and Polk, J. E., "Lanthanum Hexaboride Hollow Cathode for the Asteroid Redirect Robotic Mission 12.5 kW Hall Thruster," 34th International Electric Propulsion Conference, 2015, IEPC–2015–43.

[15]Salhi, A., Theoretical and experimental studies of orificed, hollow cathode operation, Ph.d., The Ohio State University, 1993.

[16]Mikellides, I. G., Katz, I., Goebel, D. M., and Polk, J. E., "Hollow cathode theory and experiment. II. A two-dimensional theoretical model of the emitter region," Journal of Applied Physics, Vol. 98, 2005.

[17]Chu, E. and Goebel, D. M., "High-current lanthanum hexaboride hollow cathode for 10-to-50-kW hall thrusters," IEEE Transactions on Plasma Science, Vol. 40, No. 9, 2012, pp. 2133–2144.

[18]Wilbur, P. J., "Ion and Advanced Electric Thruster Research," Tech. Rep. CR-165253, NASA, 1980.

[19]Friedly, V. J., "Hollow Cathode Operation at High Discharge Currents," 1990, M.Sc.

[20]Fearn, D. G. and Patterson, S. W., "Characterisation of the high current hollow cathode for the T6 thruster," 34th AIAA/ASME/SAE/ASEE Joint Propulsion Conference & Exhibit, 1998.

[21]Patterson, S. W. and Fearn, D. G., "The Generation of High Energy Ions in Hollow Cathode Discharges," 26th International Electric Propulsion Conference, 1999, pp. 695–702, IEPC-1999-125.

[22]Domonkos, M. T., Evaluation of low-current orificed hollow cathodes, Ph.d., University of Michigan, 1999.

[23]Mikellides, I. G., "Effects of Viscosity in a Partially Ionized Channel Flow with Thermionic Emission," Physics of Plasmas, Vol. 16, 2009.

[24]Polk, J., Grubisic, A., Taheri, N., Goebel, D. M., and Hornbeck, S. E., "Emitter Temperature Distributions in the NSTAR Discharge Hollow Cathode," 41st AIAA/ASME/SAE/ASEE Joint Propulsion Conference & Exhibit, 2005, AIAA-2005-4398.

[25]Goebel, D. M. Jameson, K. K. and Katz, I., "Hollow Cathode and Keeper-Region Plasma Measurements Using Ultra-Fast Miniature Scanning Probes," 40th AIAA/ASME/SAE/ASEE Joint Propulsion Conference & Exhibit, 2004, AIAA-2004-3430.

[26]Mikellides, I. G., Katz, I., Goebel, D. M., Polk, J. E., and Jameson, K. K., "Plasma processes inside dispenser hollow cathodes," Physics of Plasmas, Vol. 13, 2006.

[27]James, G., Witten, D., Hastie, T., and Tibshirani, R., An Introduction to Statistical Learning, Springer, 2013, p.66.

[28]Albertoni, R., Pedrini, D., Paganucci, F., and Andrenucci, M., "A Reduced-Order Model for Thermionic Hollow Cathodes," IEEE Transactions on Plasma Science, Vol. 41, No. 7, 2013, pp. 1731–1745.

[29]Goebel, D. and Katz, I., Fundamentals of Electric Propulsion: Ion and Hall Thrusters, John Wiley & Sons, Inc., 2008.

[30]Siegfried, D. E. and Wilbur, P. J., "A model for mercury orificed hollow cathodes - Theory and experiment," AIAA journal, Vol. 22, No. 10, 1984, pp. 1405–1412.

[31]Lidsky, L. M., Rothleder, S. D., Rose, D. J., Yoshikawa, S., Michelson, C., and Mackin Jr., R. J., "Highly ionized hollow cathode discharge," Journal of Applied Physics, Vol. 33, 1962, pp. 2490–2497.

[32]Delcroix, J.-L. and Trindade, A. R., "Hollow cathode arcs," Advances in Electronics and Electron Physics, Vol. 35, 1974, pp. 87–190.

[33]Siegfried, D. E. and Wilbur, P. J., "Studies on an experimental quartz tube hollow cathode," 14th International Electric Propulsion Conference, 1979.

[34]Rohrbach, G. and Lunk, A., "Characterization of plasma conditions in a hollow cathode arc evaporation device," Surface and Coatings Technology, Vol. 123, 2000, pp. 231–238.

[35]Pedregosa, F., Varoquaux, G., Gramfort, A., Michel, V., Thirion, B., Grisel, O., Blondel, M., Prettenhofer, P., Weiss, R., Dubourg, V., Vanderplas, J., Passos, A., Cournapeau, D., Brucher, M., Perrot, M., and Duchesnay, E., "Scikit-learn: Machine Learning in Python," Journal of Machine Learning Research, Vol. 12, 2011, pp. 2825–2830.

[36]Anderson, T. V. and Mattson, C. A., "Propagating Skewness and Kurtosis Through Engineering Models for Low-Cost, Meaningful, Nondeterministic design," Journal of Mechanical Design, Vol. 134, 2012, pp. 100911–1 – 100911–9.

Appendix

Correlation coefficients

Species	Quantity	Index		
		0	1	2
Xe	T_{eV}	1.3	0.34	0.48
	L_{emit}	0.75	1.0	3.0
Ar	T_{eV}	1.91	0.341	0.945
	L_{emit}	0.86	0.613	1.89

Table 1: The coefficients used for the insert electron temperature and attachment length correlations (Eqns. 6 and 7).

Expansion of functions of a random variable

Theorem 1. *If X is a random variable that follows a normal distribution of mean μ_X and variance σ_X^2 ($X \sim \mathcal{N}\left(\mu_X, \sigma_X^2\right)$) and $f : X \mapsto f(X)$ is an arbitrary function then the mean of $f(X)$ is given by*

$$\begin{aligned}\mathbb{E}\left[f(X)\right] = &\sum_{n=0}^{N-1} \frac{\sigma_X^{2n}\,(2n-1)!!}{(2n)!} f^{(2n)}(\mu_X) \\ &+ \mathcal{O}\left(\frac{\sigma_X^{2N}\,(2N-1)!!}{(2N)!} f^{(2N)}(\mu_X)\right)\end{aligned} \tag{9}$$

Proof. The Taylor expansion of $f(X)$ around μ_X is given by

$$\begin{aligned}f(X) = &\sum_{k=0}^{N-1} \frac{1}{k!} f^{(k)}(\mu_X)\,(X-\mu_X)^k \\ &+ \mathcal{O}\left(\frac{1}{N!} f^{(N)}(\mu_X)\,(X-\mu_X)^N\right).\end{aligned}$$

The expected value of the sum is the sum of expected values:

$$\begin{aligned}\mathbb{E}\left[f(X)\right] = &\sum_{k=0}^{N-1} \frac{1}{k!} f^{(k)}(\mu_X)\,\mathbb{E}\left[(X-\mu_X)^k\right] \\ &+ \mathcal{O}\left(\frac{1}{N!} f^{(N)}(\mu_X)\,\mathbb{E}\left[(X-\mu_X)^N\right]\right)\end{aligned}$$

Because $X \sim \mathcal{N}\left(\mu_X, \sigma_X^2\right)$ its odd moments are zero:

$$\forall k = 2n+1, n \in \mathbb{N}, \mathbb{E}\left[(X-\mu_X)^k\right] = 0,$$

and its even moments are given by

$$\forall k = 2n, n \in \mathbb{N}, \mathbb{E}\left[(X-\mu_X)^k\right] = \sigma_X^k\,(k-1)!!$$

Replacing the k-th order moment with the two previous formulas in the Taylor expansion for the expected value yields the theorem for the expected value of $f(X)$. □

Theorem 2. *If X is a random variable that follows a normal distribution of mean μ_X and variance σ_X^2 ($X \sim \mathcal{N}\left(\mu_X, \sigma_X^2\right)$) and $f : X \mapsto f(X)$ is an arbitrary function then the variance of $f(X)$ is approximated by*

$$\text{Var}\left[f(X)\right] \approx \sigma_X^2 \left(f^1(\mu_X)\right)^2 + \frac{1}{2}\left(f^2(\mu_X)\right)^2 \sigma_X^4 \tag{10}$$

Proof. See Ref. 36 □

Lemma 1. *If X is a random variable that follows a normal distribution of non-zero mean μ_X and variance σ_X^2 and $\sigma_X/\mu_X \ll 1$, then $Y = \ln X$ can be approximated as a normal distribution of mean $\mu_Y = \ln \mu_X - \sigma_X^2/2$ and variance $\sigma_Y^2 = \sigma_X^2/\mu_X^2$. The truncation error for the mean is equal to $3/4\,(\sigma_X/\mu_X)^4$.*

Lemma 2. *If X is a random variable that follows a normal distribution of non-zero mean μ_X and variance σ_X^2 and $\sigma_X/\mu_X \ll 1$, then $Y = 1/X$ can be approximated as a normal distribution of mean $\mu_Y = 1/\mu_X \left(1 + \sigma_X^2\mu_X^2 + 3\sigma_X^4/\mu_X^4 + 15\sigma_X^6/\mu_X^6\right)$ and variance $\sigma_Y^2 = \sigma_X^2/\mu_X^2$. The truncation error for the mean is equal to $105\sigma_X^8/\mu_X^9$.*

Proof. This is a direct application of Theorems 1 and 2 where $f(X) = \ln X$ and $f(X) = 1/X$ □

Validity of approximations

Because of the increasing value of the moments of a normal distribution the truncation error of the expected value for both $\ln X$ and $1/X$ grows without bounds. We retain only the first few terms for the above approximations. The approximations are valid as long as $\sigma_X/\mu_X \ll 1$ and μ_X is non-zero.